

RESEARCH

Open Access



# The therapeutic utility of combining dynamic contrast-enhanced magnetic resonance imaging with arterial spin labeling in the staging of nasopharyngeal carcinoma

Haodong Li<sup>1,2</sup>, Guanzhong Gong<sup>2</sup>, Lizhen Wang<sup>2</sup>, Ya Su<sup>2</sup>, Jie Lu<sup>2</sup> and Yong Yin<sup>2\*</sup>

## Abstract

**Background** To research the pathological and clinical staging uses of arterial spin labeling (ASL) and dynamic contrast-enhanced magnetic resonance imaging (DCE-MRI).

**Materials and methods** 64 newly diagnosed nasopharyngeal carcinoma (NPC) patients were enrolled from December 2020 to January 2022, and 3.0 T MRI (Discovery 750W, GE Healthcare, USA) were used for ASL and DCE-MRI scans. The DCE-MRI and ASL raw data were processed post-acquisition on the GE image processing workstation (GE Healthcare, ADW 4.7, USA). The volume transfer constant (Ktrans), blood flow (BF), and accompanying pseudo-color images were generated automatically. Draw the region of interest (ROIs), and the Ktrans and BF values for each ROI were recorded separately. Based on pathological information and the most recent AJCC staging criteria, patients were divided into low T stage groups = T<sub>1-2</sub> and high T stage groups = T<sub>3-4</sub>, low N stage groups = N<sub>0-1</sub> and high N stage groups = N<sub>2-3</sub>, and low AJCC stage group = stage I-II and high AJCC stage group = stage III-IV. The association between the Ktrans<sub>t</sub> and BF parameters and the T, N, and AJCC stages was compared using an independent sample t-test. Using a receiver operating characteristic (ROC) curve, the sensitivity, specificity, and AUC of Ktrans<sub>t</sub>, BF<sub>t</sub>, and their combined use in T and AJCC staging of NPC were investigated and assessed.

**Result** The tumor-BF (BF<sub>t</sub>) (t = - 4.905, P < 0.001) and tumor-Ktrans (Ktrans<sub>t</sub>) (t = - 3.113, P = 0.003) in the high T stage group were significantly higher than those in the low T stage group. The Ktrans<sub>t</sub> in the high N stage group was significantly higher than that in the low N stage group (t = - 2.071, P = 0.042). The BF<sub>t</sub> (t = - 3.949, P < 0.001) and Ktrans<sub>t</sub> (t = - 4.467, P < 0.001) in the high AJCC stage group were significantly higher than those in the low AJCC stage group. BF<sub>t</sub> was moderately positively correlated with the T stage (r = 0.529, P < 0.001) and AJCC stage (r = 0.445, P < 0.001). Ktrans<sub>t</sub> was moderately positively correlated with T staging (r = 0.368), N staging (r = 0.254), and AJCC staging (r = 0.411). There was also a positive correlation between BF and Ktrans in gross tumor volume (GTV) (r = 0.540, P < 0.001), parotid (r = 0.323, P < 0.009) and lateral pterygoid muscle (r = 0.445, P < 0.001). The sensitivity of the combined application of Ktrans<sub>t</sub> and BF<sub>t</sub> for AJCC staging increased from 76.5 and 78.4 to 86.3%, and the AUC value increased from 0.795 and 0.819 to 0.843, respectively.

**Conclusion** Combining Ktrans and BF measures may make it possible to identify the clinical stages in NPC patients.

**Keywords** DCE-MRI, Arterial spin labeling, Nasopharyngeal carcinoma, Clinical staging

\*Correspondence:

Yong Yin

yinyongsd@126.com

Full list of author information is available at the end of the article



© The Author(s) 2023. **Open Access** This article is licensed under a Creative Commons Attribution 4.0 International License, which permits use, sharing, adaptation, distribution and reproduction in any medium or format, as long as you give appropriate credit to the original author(s) and the source, provide a link to the Creative Commons licence, and indicate if changes were made. The images or other third party material in this article are included in the article's Creative Commons licence, unless indicated otherwise in a credit line to the material. If material is not included in the article's Creative Commons licence and your intended use is not permitted by statutory regulation or exceeds the permitted use, you will need to obtain permission directly from the copyright holder. To view a copy of this licence, visit <http://creativecommons.org/licenses/by/4.0/>. The Creative Commons Public Domain Dedication waiver (<http://creativecommons.org/publicdomain/zero/1.0/>) applies to the data made available in this article, unless otherwise stated in a credit line to the data.

## Background

Nasopharyngeal carcinoma (NPC) has the highest rate of tumors of the head and neck in Southeast Asia [1, 2]. Radiotherapy is the main treatment for NPC [3, 4]. For the individualization of treatment and the forecasting of patient outcomes, accurate clinical staging before therapy is essential. Since MRI has the highest resolution of soft tissue and the highest sensitivity for NPC identification, it has been the preferred imaging modality for NPC staging [5]. Unfortunately, morphology-based imaging methods cannot detect tumor microbiological information. As a result, it might compromise the precision of NPC staging.

Traditional anatomy-based imaging methods may have evaluation errors [6], therefore the MR functional pictures based on dynamic contrast-enhanced magnetic resonance imaging (DCE-MRI) and arterial spin labeling (ASL) are crucial for determining the effectiveness of treatment for NPC, staging accurately, and other purposes [7].

Exogenous Gd-contrast agents are required for DCE-MRI. It accumulates in the extracellular space, which is dictated by tissue perfusion, capillary permeability, and surface area, and it may perform visual or semi-quantitative analysis [8, 9]. DCE-MRI can collect a variety of information on tissue perfusion, including the ability to objectively measure capillary permeability, NPC perfusion, tumor hypoxia, and tumor biological activity using temporal signal intensity curves [10]. When compared to the role of MR anatomical images in the diagnosis of NPC, DCE-MRI can further improve the capacity of diagnosis, differential diagnosis, and precise staging.

Unlike DCE-MRI perfusion, ASL is fully non-invasive and does not require an injection of a contrast agent. Using magnetically tagged water protons from arterial blood as an endogenous tracer, this method creates images that can show microscopic modifications such as tissue blood perfusion and micro-vessel density [11]. ASL's primary physiological parameter is blood flow (BF), which determines the rate at which oxygen and nutrients are transported to the capillary bed and provides physiological information on tissue blood perfusion [12].

These two techniques have been utilized to stage NPC and predict therapy response or prognosis [5, 7, 13]. As a result, the combination of ASL and DCE-MRI is promising for reflecting the type of NPC and has the potential to improve staging accuracy. In this study, the two imaging techniques DCE-MRI and ASL were used to stage NPC to investigate the function of DCE-MRI and ASL in determining the staging of NPC.

## Materials and methods

The Shandong Cancer Hospital Medical Ethics Committee approved the study (NO. SDTHEC2022006002). Before the MR examination, all patients provided informed consent and signed. 77 newly diagnosed NPC patients underwent MRI scans between December 2020 and January 2022. Due to the image quality of conventional sequences will be affected by noise, motion artifacts, and metal foreign body artifacts created by patients during MR testing, there were no artifacts in either the ASL or DCE-MRI scans and 13 patients were excluded. Finally, 64 patients were included. All participants in this study met the requirements listed below:

- (a) Biopsy-proven diagnosis of NPC;
- (b) No history of prior chemotherapy, radiotherapy, or other treatments;
- (c) No contraindications for MR examination;
- (d) No concurrent nasopharyngeal disease or other tumors.

Exclusion criteria:

- (a) patients with recurrent NPC after treatment;
- (b) MR image quality is poor (noise, motion artifacts, and metallic foreign body artifacts are the main causes), as long as there are artifacts visible in each sequence image, the image does not meet the requirements.

The pathology diagnosis for all individuals was NPC which was either poorly differentiated or undifferentiated. There were 64 patients (45 males and 19 women; mean age, 51 years; range, 14–80 years). The American Joint Committee on Cancer (AJCC) staging approach was used for the tumor, node, and metastasis TNM staging. Together with their clinical demographic information, the distribution of each patient's individual AJCC and TNM stages are listed in Table 1.

## MR imaging protocol

The 3.0 T MRI (Discovery 750W, GE Healthcare, USA) Scanner was used for all of the patients' MRI scans. Supine MR scanning specifications: all patients were scanned from the clavicle to the superior edge of the frontal sinus. Six-channel head and neck coils were used. The imaging protocol included the following: (1) axial T1 weighted images (fast spin echo, FSE): repetition time/echo time (TR/TE)=8.5/3.2 ms, thickness=3 mm, slice gap=1 mm, field of view (FOV)=25.6 cm, matrix=256 × 256; (2) axial T2-weighted images (fast spin echo, FSE): TR/TE=13,500/114 ms,

**Table 1** Clinical characteristics of 64 patients

Parameters	Results (%)
Sex(male/female)	45(70%)/19(30%)
Age(years)	51
Range(years)	14–80
T stage	
T1	9(14%)
T2	23(36%)
T3	22(34%)
T4	10(16%)
N stage	
N0	9(14%)
N1	16(25%)
N2	17(27%)
N3	22(34%)
M stage	
M0	63(98%)
M1	1(2%)
AJCC stage	
I	0(0%)
II	13(20%)
III	23(36%)
IV	28(44%)

AJCC American Joint Committee on Cancer

thickness=3 mm, slice gap=1 mm, FOV=26 cm, matrix=416 × 416; (3) axial T2 with fat suppression (fast recovery fast spin echo, FRFSE): TR/TE = 11,000/114 ms, thickness=3 mm, slice gap=1 mm, FOV=28 cm, matrix=320 × 320; (4) axial ASL (3D fast spin echo spiral-based pseudo-continuous ASL sequence): TR/TE = 5160/11.5 ms, NEX=3, bandwidth=62.5 kHz, thickness=3 mm, FOV=25.6 cm, labeling duration=1500 ms, post-labeling delay=2025 ms. (5) axial DCE-MRI imaging (gradient echo sequence, GRE): TR/TE = 5.5/2.7 ms, thickness=3 mm, slice gap=0 mm, FOV=40 × 32 cm, matrix=300 × 180. An intravenous injection of 0.2 mmol/kg gadolinium acid meglumine salt (Jiangsu Hengrui Pharmaceuticals Co., Ltd. Batch number: 220519BT) was carried out at an injection rate of 3 ml/s via a power injector, followed by a flush of an equal volume of normal saline. Another ASL was acquired after the completion of DCE-MRI.

**Postprocessing and evaluation**

Two senior radiologists used MIM Maestro 6.8.8 to delineate the parotid gland, lateral pterygoid muscle, and gross tumor volume (GTV) in T2WI-FS images, which was then reviewed by a third senior radiologist. The GE image processing workstation (GE Healthcare, ADW 4.7, USA) performs post-processing on the DCE and ASL

raw data (Fig. 1). Pseudo-colored maps with the matching Ktrans and BF parameters were created automatically after being computed separately (Fig. 1B, C). Because Ktrans is the most typical metric in DCE, we solely measured it. The BF and Ktrans maps were rigidly registered to the axial T2WI-FS at a workstation using commercial software (GE Healthcare, ADW 4.7, USA) (Fig. 1D, E). The regions of interest (ROIs) were manually drawn by one radiologist with > 10 years of clinical experience in head and neck radiology. According to the pseudo-color perfusion of images, the ROIs were set at the slice with the highest perfusion signal while avoiding areas of cysts, necrosis, calcifications, hemorrhage, and large vessels. Three separate ROIs were obtained at the largest cross-section of the lesion, and the average value was taken as the final measurement result. Each ROI’s BF and Ktrans values were recorded.

A sequence with pseudo-continuous labeling, background suppression, and 3D RARE Stack-Of-Spirals readout was implemented for this study. Obtaining ASL perfusion pictures and measuring arterial blood magnetization. To eliminate physiological noise and motion artifacts, background suppression technology was applied during the image collecting procedure. After scanning, the quantitative BF maps were created automatically using the GE FuncTool 4.7 software using the following equation:

$$BF = \frac{6000\lambda(M_c - M_l) \frac{PLD}{e^{-\frac{\tau}{T_{1Blood}}}}}{2\alpha T_{1Blood} M_{PD} \left(1 - e^{-\left(\frac{\tau}{T_{1Blood}}\right)}\right)}$$

where λ is the nasopharynx/blood partition coefficient in ml/g and  $M_c$  and  $M_l$  are the time-averaged signal intensities in the control and label images respectively.  $T_{1Blood}$  is the longitudinal relaxation time of blood in seconds, α is the labeling efficiency,  $M_{PD}$  is the signal intensity of a proton density-weighted image, τ is the label duration, and PLD is the post-labeling delay.

DCE-MRI data can be analyzed using Tofts standard pharmacokinetic model, which gives the paramagnetic contrast agent (CA) concentration in tissue at time t as follows:

$$C_t(t) = K_{trans} \int_0^t C_p(\tau) e^{-\left(\frac{K_{trans}}{V_e}\right)(t-\tau)} d\tau$$

where  $V_e$  is the extravascular extracellular volume percentage,  $K_{trans}$  is the transfer rate constant, and  $C_t(t)$  is the CA concentration in arterial blood.

The patients were classified into low T stage group =  $T_{1-2}$ , high T stage group =  $T_{3-4}$ , low N stage group =  $N_{0-1}$ , high N stage group =  $N_{2-3}$ , low AJCC stage group = stage I-II, and high AJCC stage group = stage



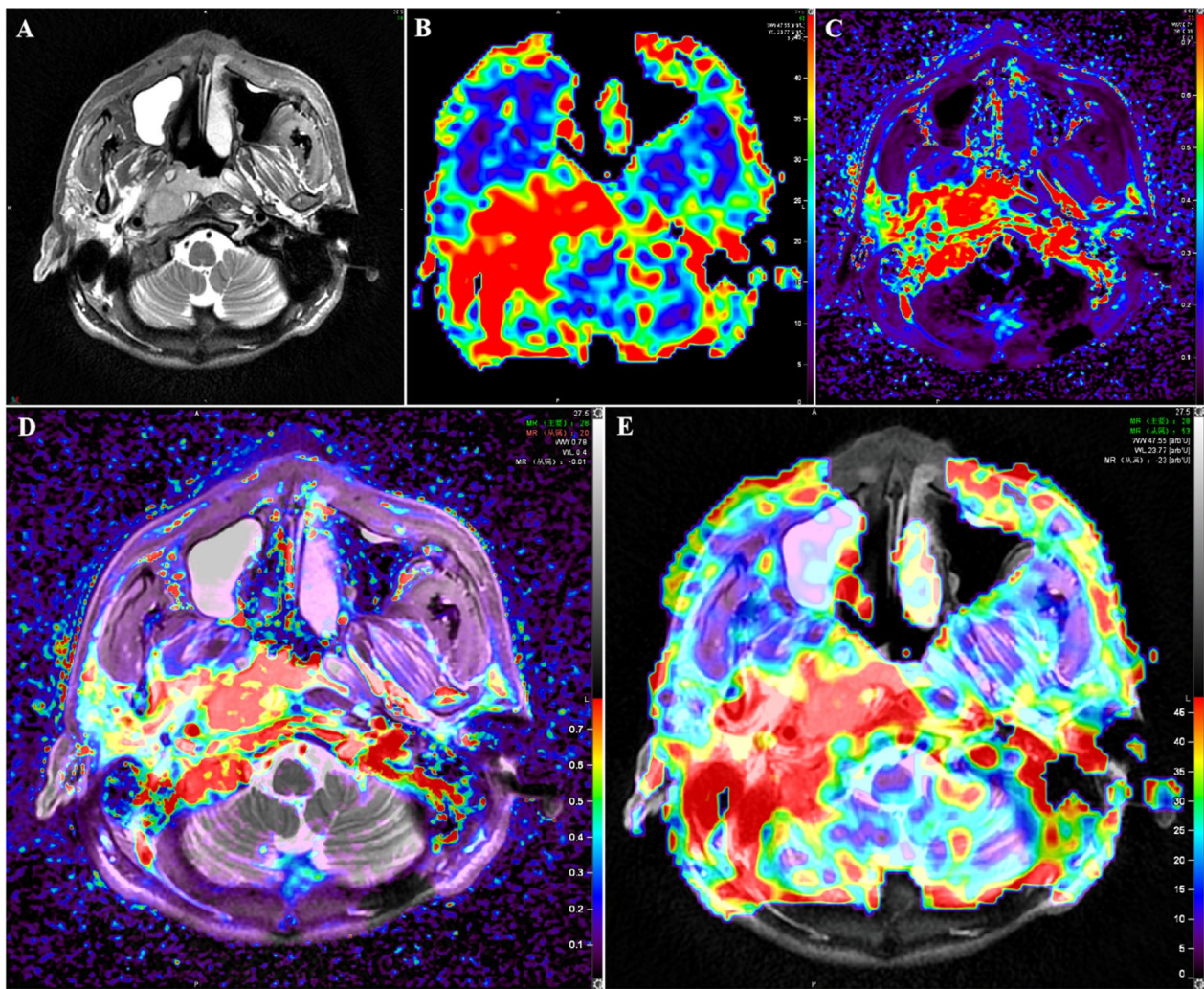


**Fig. 1** Schematic diagram of MRI of a patient. **A** T2WI-FS; **B** ASL(BF); **C** DCE-MRI(Ktrans); **D** fusion images of T2WI-FS and ASL(BF); **E** fusion images of T2WI-FS and DCE-MRI(Ktrans)

III-IV based on the pathological findings and the most recent AJCC staging criteria.

### Statistical analysis

The data were examined using SPSS (version 25.0, IBM, NY, USA), a statistical tool. Measurement data with a normal distribution are represented by the mean  $\pm$  standard deviation. The Ktrans and BF parameters of the T, N, and AJCC stages were compared using an independent sample t-test. The relationship between MRI parameters and the clinical stage was investigated using Spearman correlation analysis. To identify and assess the sensitivity, specificity, and AUC of Ktrans, BF, and their combination in T, N, and AJCC staging of NPC, the receiver operating characteristic curve (ROC) was used.

### Results

In total, 64 people with NPC were included in this study. 32 patients were in the low T stage ( $T_{1-2}$ ), and 32 people were in the high T stage ( $T_{3-4}$ ). There were 25 (39%) and 39 (61%) people with low N stage ( $N_{0-1}$ ) and high N stage, respectively ( $N_{2-3}$ ). Low AJCC stage (I-II stage) patients made up 13 (20%), while high AJCC stage (III-IV stage) patients made up 51 (80%) (Table 1).

The characteristics of the low-stage and high-stage groups are compared for DCE and ASL (Table 2). In comparison to the low T stage group,  $BF_t$  ( $t = -4.905$ ,  $P = 0.001$ ) and  $Ktrans_t$  ( $t = -3.113$ ,  $P = 0.003$ ) were significantly higher in the high T stage group.  $Ktrans_t$  was noticeably higher in the group with high N stages than in the group with low N stages ( $t = -2.071$ ,

**Table 2** Comparison of BF and Ktrans values across different clinical stages

Staging classification	Cases	BF <sub>t</sub>	Ktrans <sub>t</sub>	BF <sub>p</sub>	Ktrans <sub>p</sub>	BF <sub>l</sub>	Ktrans <sub>l</sub>
T stage							
T1 + T2	32	47.15 ± 17.94	0.79 ± 0.43	17.80 ± 5.59	0.69 ± 0.65	15.36 ± 2.80	0.21 ± 0.15
T3 + T4	32	67.56 ± 14.58	1.24 ± 0.69	15.71 ± 2.90	0.81 ± 0.58	14.81 ± 1.87	0.19 ± 0.15
<i>t</i>		- 4.905	- 3.113	1.873	- 0.789	0.926	0.495
<i>P</i>		0.000*	0.003*	0.067	0.433	0.358	0.648
N stage							
N0 + N1	25	52.92 ± 21.17	0.82 ± 0.50	17.18 ± 5.01	0.82 ± 0.70	15.23 ± 2.67	0.21 ± 0.19
N2 + N3	39	60.49 ± 17.30	1.14 ± 0.65	16.48 ± 4.26	0.70 ± 0.56	14.99 ± 2.22	0.20 ± 0.11
<i>t</i>		- 1.565	- 2.071	0.601	0.759	0.388	0.371
<i>p</i>		0.123	0.042*	0.550	0.451	0.700	0.712
AJCC stage							
I + II	13	40.70 ± 14.49	0.60 ± 0.37	18.40 ± 5.89	0.82 ± 0.87	15.64 ± 3.03	0.21 ± 0.18
III + IV	51	61.82 ± 17.81	1.12 ± 0.62	16.34 ± 4.09	0.73 ± 0.54	14.94 ± 2.21	0.20 ± 0.14
<i>t</i>		- 3.949	- 4.467	1.476	0.099	0.940	0.099
<i>p</i>		0.000*	0.000*	0.145	0.921	0.351	0.921

BF<sub>t</sub> tumor-BF; Ktrans<sub>t</sub> tumor-Ktrans; BF<sub>p</sub> parotid gland-BF; Ktrans<sub>p</sub> parotid gland-Ktrans; BF<sub>l</sub> lateral pterygoid muscle-BF; Ktrans<sub>l</sub> lateral pterygoid muscle-Ktrans  
 \*P < 0.05

**Table 3** Correlation of BF and Ktrans values with stage

Parameters	T stage	N stage	AJCC stage
BF <sub>t</sub>			
<i>r</i>	0.529	0.206	0.445
<i>P</i>	< 0.001*	0.102	< 0.001*
Ktrans <sub>t</sub>			
<i>r</i>	0.368	0.254	0.411
<i>P</i>	0.003*	0.042*	0.001*
BF <sub>p</sub>			
<i>r</i>	- 0.140	- 0.077	- 0.159
<i>P</i>	0.268	0.545	0.210
Ktrans <sub>p</sub>			
<i>r</i>	0.147	- 0.029	- 0.096
<i>P</i>	0.246	0.817	0.452
BF <sub>l</sub>			
<i>r</i>	- 0.045	- 0.015	- 0.062
<i>P</i>	0.725	0.908	0.626
Ktrans <sub>l</sub>			
<i>r</i>	- 0.107	0.088	0.026
<i>P</i>	0.402	0.492	0.837

BF<sub>t</sub> tumor-BF; Ktrans<sub>t</sub> tumor-Ktrans; BF<sub>p</sub> parotid gland-BF; Ktrans<sub>p</sub> parotid gland-Ktrans; BF<sub>l</sub> lateral pterygoid muscle-BF; Ktrans<sub>l</sub> lateral pterygoid muscle-Ktrans  
 \*P < 0.05

P = 0.042). In comparison to the low AJCC stage group, BF<sub>t</sub> (*t* = - 3.949, P = 0.001) and Ktrans<sub>t</sub> (*t* = - 4.467, P = 0.001) were considerably greater in the high AJCC stage group. Between the T, N, and AJCC staging groups, there was no statistically significant difference

in parotid gland-BF (BF<sub>p</sub>), parotid gland-Ktrans (Ktrans<sub>p</sub>), lateral pterygoid muscle-BF (BF<sub>l</sub>), or lateral pterygoid muscle-Ktrans (Ktrans<sub>l</sub>). BF<sub>t</sub> did not significantly differ in the N stage group.

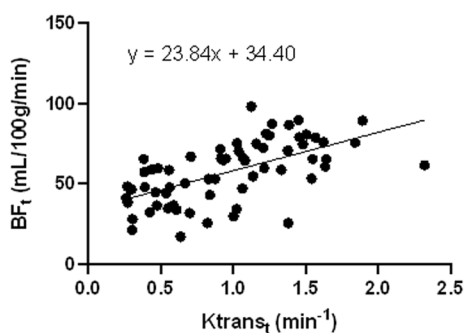
Tables 3 and 4 depicts the association between MR parameters and stage. BF<sub>t</sub> value was associated with the T stage (*r* = 0.529, P < 0.001) and AJCC stage (*r* = 0.445, P < 0.001). The T stage (*r* = 0.368, P = 0.003), N stage (*r* = 0.254, P = 0.042), and AJCC stage (*r* = 0.411, P = 0.001) were all positively correlated with the Ktrans value. Ktrans and BF had a positively correlated with the GTV (*r* = 0.540, P < 0.001), parotid gland (*r* = 0.323, P = 0.009), and lateral pterygoid muscle (*r* = 0.445, P < 0.001) (Figs. 2, 3, and 4). There was no link found between BF<sub>p</sub>, Ktrans<sub>p</sub>, BF<sub>l</sub>, and Ktrans<sub>l</sub> and AJCC stage.

Table 5 displays the sensitivity, specificity, and AUC of T staging and AJCC staging when Ktrans and BF are used alone and in combination. The AUC value was 0.806 when 50.38 mL/100 g/min was utilized as the cut-off value for the BF in the differentiation between the low and high T stages. The AUC value was 0.719 when 0.698 min<sup>-1</sup> was utilized as the cutoff value for the Ktrans

**Table 4** Correlation between the BF values of the tumor, parotid gland, and lateral pterygoid muscle and their Ktrans

	BF <sub>t</sub> -Ktrans <sub>t</sub>	BF <sub>p</sub> -Ktrans <sub>p</sub>	BF <sub>l</sub> -Ktrans <sub>l</sub>
<i>r</i>	0.540	0.323	0.445
<i>P</i>	< 0.001*	0.009*	< 0.001*

BF<sub>t</sub> tumor-BF; Ktrans<sub>t</sub> tumor-Ktrans; BF<sub>p</sub> parotid gland-BF; Ktrans<sub>p</sub> parotid gland-Ktrans; BF<sub>l</sub> lateral pterygoid muscle-BF; Ktrans<sub>l</sub> lateral pterygoid muscle-Ktrans  
 \*P < 0.05



**Fig. 2** Scatterplot of  $BF_t$  and  $Ktrans_t$ . There was a moderate positive correlation between BF and Ktrans in the tumor area

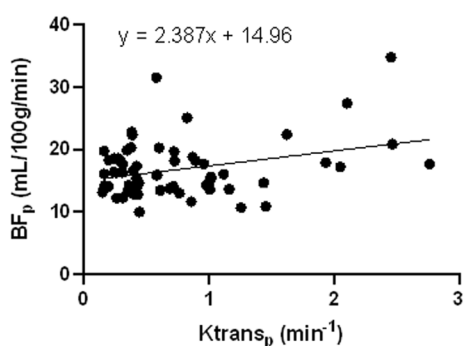


**Fig. 3** Scatterplot of  $BF_p$  and  $Ktrans_p$ . There was a moderate positive correlation between BF and Ktrans in the parotid gland

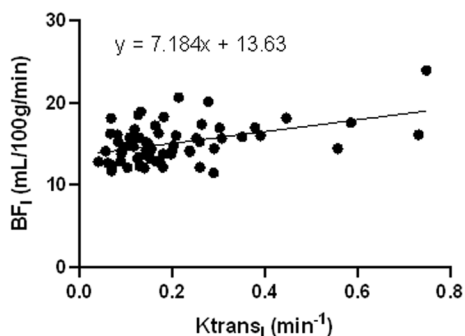


**Fig. 4** Scatterplot of  $BF_l$  and  $Ktrans_l$ . There was a moderate positive correlation between BF and Ktrans in the Lateral pterygoid muscle

in the differentiation between the low and high T stage. The combination of  $Ktrans$  and BF had AUC values of 0.808. There was no statistically significant difference in AUC values ( $P > 0.05$ ). The AUC value was 0.819 when 48.10 mL/100 g/min was utilized as the cutoff value for BF in the distinction of low and high AJCC stage. The AUC value was 0.795 when  $0.698 \text{ min}^{-1}$  was utilized as the cutoff value for the  $Ktrans$  in the distinction of low and high AJCC stage. The combination of  $Ktrans$  and BF had AUC values of 0.843. There was no statistically significant difference in AUC values ( $P > 0.05$ ) (Figs. 5 and 6).

**Discussion**

ASL and DCE were employed alone or in combination to assess the clinical stage of NPC in this investigation. BF and  $Ktrans$  were found to be useful in distinguishing between high and low T stages and high and low AJCC stages, with a substantial connection. The combination of ASL and DCE is more effective than either alone for the accurate staging of NPC.

By using data on blood perfusion and capillary permeability, DCE-MRI and ASL can both assist in determining the stage of NPC. According to recent studies, high T stage and high AJCC stage tumors showed higher BF values than low T stage and low AJCC stage cancers [14]. Sriyook et al.'s [15] research revealed a significant difference in  $Ktrans$  between the low T and high T stage. We found that the  $BF_t$  and  $Ktrans_t$  of the high T stage were higher than those of the low T stage. With increasing T stage, the tumor region's capillary permeability and blood perfusion increased, and the high T stage tumor cells were more active than the low T stage tumor cells. There was no discernible variation in the  $BF_t$  value even though the  $Ktrans_t$  of the high N stage was slightly higher than that of the low N stage. We believe that this parameter has no bearing on the lymph node metastasis of NPC and that the metastasis may only be marginally impacted by the blood supply of the tumor site.

It was recently discovered that the mean values of  $Ktrans$ , rate constant ( $K_{ep}$ ), and blood plasma volume ( $V_p$ ) in the III-IV stages were much greater than those in the I-II stages.  $Ktrans$ ,  $K_{ep}$ , and  $V_p$  were found to be strongly linked with tumor stage using univariate

**Table 5** Diagnostic sensitivity and specificity of NPC T and AJCC staging using  $BF_t$  and  $Ktrans_t$  alone or in combination

Parameters	T stage			AJCC stage		
	Sensitivity (%)	Specificity (%)	AUC	Sensitivity (%)	Specificity (%)	AUC
$BF_t$	90.6	65.6	0.806	78.4	84.6	0.819
$Ktrans_t$	84.4	56.3	0.719	76.5	84.6	0.795
$BF_t + Ktrans_t$	90.6	65.6	0.808	86.3	76.9	0.843

NPC nasopharyngeal carcinoma; AJCC American Joint Committee on Cancer;  $Ktrans_t$  volume transfer constant;  $BF_t$  tumor blood flow



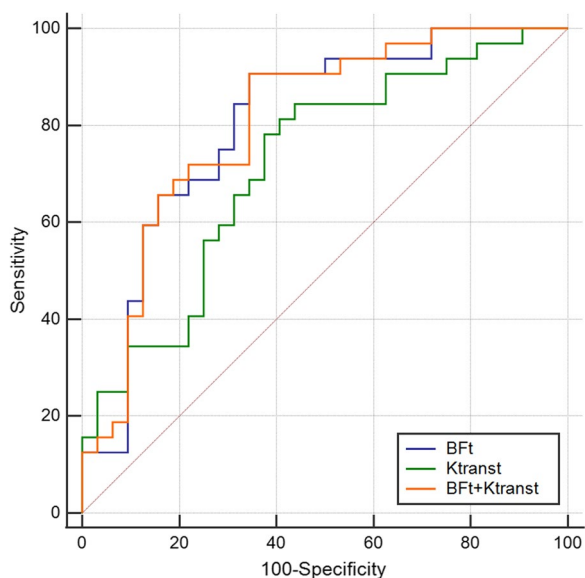


**Fig. 5** ROC curve analysis for T staging of NPC using the  $BF_t$ ,  $Ktranst$ , and both in combination. The AUCs of the  $BF_t$ ,  $Ktranst$ , and  $BF_t + Ktranst$  were 0.806, 0.719, and 0.808, respectively.  $BF_t + Ktranst$  achieved the highest AUC

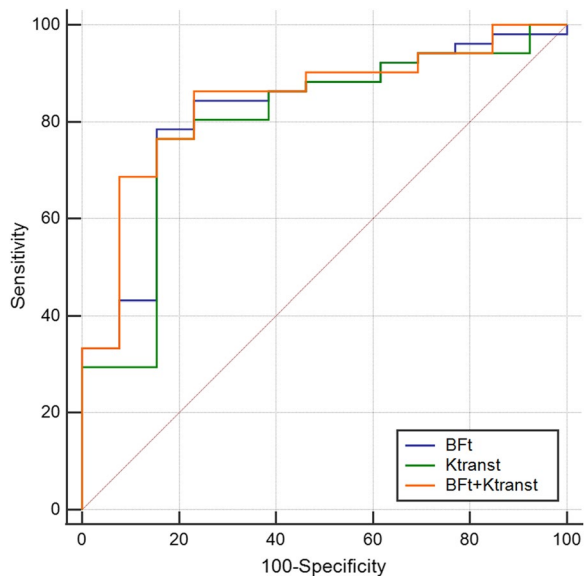


**Fig. 6** ROC curve analysis for AJCC staging of NPC using the  $BF_t$ ,  $Ktranst$ , and both in combination. The AUCs of the  $BF_t$ ,  $Ktranst$ , and  $BF_t + Ktranst$  were 0.819, 0.795, and 0.843, respectively.  $BF_t + Ktranst$  achieved the highest AUC

logistic regression analysis [16]. Our research came to a similar conclusion. The  $Ktranst$  and  $BF_t$  of the high AJCC stage were significantly greater than those of the low AJCC stage. The high-stage tumors differ from low-stage tumors in that they spread more quickly,

grow more invasively, and require larger blood flow to provide nourishment and oxygen to the tumor location. DCE-MRI and ASL can therefore predict the clinical stage of NPC by assessing BF and Ktrans. The Ktrans and BF values for the lateral pterygoid muscle and parotid gland in each stage group did not significantly change. Because the majority of the patients we recruited were at stage M0, the tumor did not invade the parotid gland or the lateral pterygoid muscle. As a result, tumor size, depth of invasion, and lymph node metastasis may not have a substantial effect on BF and Ktrans that OARs.

According to some studies, a strong correlation between ASL and DCE-MRI in the perfusion of NPC [17]. According to Zheng et al., Ktrans had a moderately negative correlation with UICC staging, T staging, and N staging ( $r = -0.447$ ,  $r = -0.244$ , and  $r = -0.247$ , respectively) [18]. Researchers Sriyook Aniwat et al. found a correlation between plasma EBV-DNA levels and NPC stages and DCE-MRI features. Ktrans and T stage had the greatest correlation coefficient. The high T stage (T3-T4), low T stage (T1-T2), low AJCC stage (I-II stage), and high AJCC stage (III-IV stage) may all be distinguished with accuracy by Ktrans [15]. In this study, it was also found that, with the exception of the N stage, T and AJCC stages were moderately positively linked with  $BF_t$ , whereas T, N, and AJCC stages were moderately positively linked with  $Ktranst$ . In the parotid gland, lateral pterygoid muscle, and tumor region, Ktrans and BF were correlated. While BF mainly reflected blood perfusion, Ktrans mainly indicated increased new capillary permeability, which led to higher blood perfusion. The high stage tumors were more permeable to neovascularization, their tumor foci had an ample blood supply, and more contrast media accumulated. In comparison to tumor tissue, there was also a correlation between BF and Ktrans in normal tissue (parotid gland and lateral pterygoid muscle), which implied that the higher the capillary permeability was in the place of high blood perfusion in normal tissue. However, the tumor did not infiltrate the parotid gland or the lateral pterygoid muscle, and blood perfusion and capillary permeability were normal, thus the majority of them were in low BF and low Ktrans locations (Figs. 2, 3, and 4). Combining DCE-MRI with ASL analysis may help in the study of vascular permeability and blood perfusion in NPC. It can be applied as an extra measurement to evaluate tumor blood flow, stage the tumor, and provide a qualitative NPC diagnosis.

When used together, ASL and DCE-MRI can improve the diagnostic accuracy of MRI in the grading and staging of brain tumors, parotid tumor subtype distinction, and NPC [19–21]. The results of this study’s ROC analysis showed that combining Ktrans and BF produced

staging results for T and AJCC that were more precise than either method used alone. The AJCC staging's AUC outperformed T staging by a wide margin. Combination detection has a significantly higher sensitivity than solo detection for AJCC staging. The stage of the tumor may be more accurately determined if Ktrans and BF are detected simultaneously.

This research has some limitations. To begin with, the sample size is small. Because of the small sample size and the small number of people in the M1 stage, there is no statistical analysis of the M stage. In the future, we plan to collect more data on patients with NPC, particularly those with distant metastasis, to undertake additional studies. Second, Ktrans is the most commonly utilized in clinical settings and is the most representative of DCE [22]. Therefore, our study only looks at how the Ktrans parameters and BF relate to one another. In upcoming research, the relationship between ASL (BF) and other DCE parameters ( $V_e$ ,  $K_{ep}$ ,  $V_p$ , etc.) will be further discussed.

## Conclusions

In conclusion, Ktrans values acquired from DCE-MRI combined with BF values derived from ASL might be utilized to assess capillary permeability and perfusion of NPC and offer helpful data for assessing stages in NPC patients.

## Abbreviations

ASL	Arterial spin labeling
DCE-MRI	Dynamic-contrast-enhanced magnetic resonance imaging
MRI	Magnetic resonance imaging
Ktrans	Volume transfer constant
$K_{ep}$	Rate constant
$V_p$	Blood plasma volume
NPC	Nasopharyngeal carcinoma
AJCC	American Joint Committee on Cancer
BF	Blood flow
ROC	Receiver operating characteristic curve
T1WI	T1 weighted images
T2WI	T2 weighted images
T2WI-FS	T2 weighted fat suppression imaging
TR	Repetition time
TE	Echo time
FOV	Field of view
ROI	Region of interest
OAR	Organs at risk
EBV-DNA	Epstein-Barr virus DNA
GTV	Gross tumor volume
AUC	Area under curve
MR	Magnetic resonance
UICC	International Union Against Cancer

## Acknowledgements

We thank all members of the Radiophysics Technology Department of the affiliated Cancer Hospital of Shandong First Medical University for helpful discussions and invaluable help in manuscript preparation.

## Author contributions

HDL (study concepts and design, data acquisition, data analysis, manuscript draft, and editing); GZG (study concepts and design, data acquisition, manuscript draft, and editing); YS (data acquisition, data analysis); LZW (data acquisition, data analysis); JL (manuscript draft and editing, supervision of the research group). YY (study concepts and design, data analysis, manuscript draft and editing, supervision of the research group). All authors read and approved the final manuscript.

## Funding

This study was supported by the Start-up fund of Shandong Cancer Hospital (YYPY2020-016), the Key Research and Development Program of Shandong Major Science & Technology Innovation Project (2021SFGC0501), and the Natural Science Foundation of Shandong Province (ZR2020MH227). The funding body played no role in the design of the study and collection, analysis, interpretation of data, and in writing the manuscript.

## Availability of data and materials

The datasets used and analyzed during this study are available from the corresponding author upon reasonable request. The data are not publicly available due to information that could compromise the privacy of research participants.

## Declarations

### Ethics approval and consent to participate

The relevant data and images in the manuscript have obtained the informed consent of the patient or legal guardian. The study was approved by the Institutional Review Board of Shandong Cancer Hospital and was performed in compliance with the principles of the World Medical Association Declaration of Helsinki, revised in 2000, Edinburgh. Written informed consent was obtained from patients prior to MR imaging.

### Consent for publication

Not applicable.

### Competing interests

The authors declare no competing interests.

### Author details

<sup>1</sup>Department of Graduate, Shandong First Medical University (Shandong Academy of Medical Sciences), Jinan 250000, China. <sup>2</sup>Department of Radiation Physics, Shandong Cancer Hospital and Institute, Shandong First Medical University and Shandong Academy of Medical Sciences, Jinan 250117, China.

Received: 11 November 2022 Accepted: 19 April 2023

Published online: 03 May 2023

## References

- Chen YP, Chan ATC, Le QT, Blanchard P, Sun Y, Ma J. Nasopharyngeal carcinoma. *Lancet*. 2019;394(10192):64–80. [https://doi.org/10.1016/S0140-6736\(19\)30956-0](https://doi.org/10.1016/S0140-6736(19)30956-0).
- Chang ET, Ye W, Zeng YX, Adami HO. The evolving epidemiology of nasopharyngeal carcinoma. *Cancer Epidemiol Biomarkers Prev*. 2021;30(6):1035–47.
- Yeh SA, Hwang TZ, Wang CC, Yang CC, Lien CF, Wang CC, Hsu TY, Hsu RF, Shih YC, Huang YC, Hsieh MC, Gau JS, Chang L, Lee TF. Outcomes of patients with nasopharyngeal carcinoma treated with intensity-modulated radiotherapy. *J Radiat Res*. 2021;62(3):438–47.
- Li K, Li C, Zhu T, et al. Dosimetry study of nasopharyngeal carcinoma based on Halcyon accelerator fixed-field intensity-modulated radiation therapy. *J Cancer Res Ther*. 2021;17(5):1165–71.
- Liu L, Hu L, Zeng Q, et al. Dynamic contrast-enhanced MRI of nasopharyngeal carcinoma: correlation of quantitative dynamic contrast-enhanced magnetic resonance imaging (DCE-MRI) parameters with hypoxia-inducible factor 1 $\alpha$  expression and tumor grade/stage. *Ann Palliat Med*. 2021;10(2):2238–53.



6. What is an MRI scan and what can it do?. *Drug Ther Bull.* 2011;49(12):141–144.
7. Mui AWL, Lee AWM, Lee VHF, et al. Prognostic and therapeutic evaluation of nasopharyngeal carcinoma by dynamic contrast-enhanced (DCE), diffusion-weighted (DW) magnetic resonance imaging (MRI) and magnetic resonance spectroscopy (MRS). *Magn Reson Imaging.* 2021;83:50–6.
8. Umamura Y, Wang D, Peck KK, et al. DCE-MRI perfusion predicts pseudoprogression in metastatic melanoma treated with immunotherapy. *J Neurooncol.* 2020;146(2):339–46.
9. Abreu-Gomez J, Lim C, Cron GO, Krishna S, Sadoughi N, Schieda N. Pharmacokinetic modeling of dynamic contrast-enhanced (DCE)-MRI in PI-RADS category 3 peripheral zone lesions: preliminary study evaluating DCE-MRI as an imaging biomarker for detection of clinically significant prostate cancers. *Abdom Radiol (NY).* 2021;46(9):4370–80.
10. Song J, Gu Y, Du T, Liu Q. Analysis of quantitative and semi-quantitative parameters of DCE-MRI in differential diagnosis of benign and malignant cervical tumors. *Am J Transl Res.* 2021;13(11):12228–34.
11. Hernandez-Garcia L, Aramendía-Vidaurreta V, Bolar DS, et al. Recent technical developments in ASL: a review of the state of the art. *Magn Reson Med.* 2022;88(5):2021–42.
12. Madhuranthakam AJ, Yuan Q, Pedrosa I. Quantitative methods in abdominal MRI: perfusion imaging. *Top Magn Reson Imaging.* 2017;26(6):251–8.
13. Liu J, Zhu J, Wang Y, et al. Arterial spin labeling of nasopharyngeal carcinoma shows early therapy response. *Insights Imaging.* 2022;13(1):114.
14. Xiao B, Wang P, Zhao Y, Liu Y, Ye Z. Combination of diffusion-weighted imaging and arterial spin labeling at 3.0 T for the clinical staging of nasopharyngeal carcinoma. *Clin Imaging.* 2020;66:127–32.
15. Sriyook A, Lertbutsayanukul C, Jittapiromsak N. Value of dynamic contrast-enhanced magnetic resonance imaging for determining the plasma Epstein-Barr virus status and staging of nasopharyngeal carcinoma. *Clin Imaging.* 2021;72:1–7.
16. Guo N, Zeng W, Deng H, et al. Quantitative dynamic contrast-enhanced MR imaging can be used to predict the pathologic stages of oral tongue squamous cell carcinoma. *BMC Med Imaging.* 2020;20(1):117.
17. Lin M, Yu X, Luo D, et al. Investigating the correlation of arterial spin labeling and dynamic contrast enhanced perfusion in primary tumor of nasopharyngeal carcinoma. *Eur J Radiol.* 2018;108:222–9.
18. Zheng D, Chen Y, Chen Y, et al. Dynamic contrast-enhanced MRI of nasopharyngeal carcinoma: a preliminary study of the correlations between quantitative parameters and clinical stage. *J Magn Reson Imaging.* 2014;39(4):940–8.
19. Hales PW, d'Arco F, Cooper J, et al. Arterial spin labelling and diffusion-weighted imaging in paediatric brain tumors. *Neuroimage Clin.* 2019;22:101696.
20. Razek AAKA. Arterial spin labelling and diffusion-weighted magnetic resonance imaging in differentiation of recurrent head and neck cancer from post-radiation changes. *J Laryngol Otol.* 2018;132(10):923–8.
21. Razek AAKA. Multi-parametric MR imaging using pseudo-continuous arterial-spin labeling and diffusion-weighted MR imaging in differentiating subtypes of parotid tumors. *Magn Reson Imaging.* 2019;63:55–9.
22. Weber JD, Spiro JE, Scheffler M, et al. Reproducibility of dynamic contrast enhanced MRI derived transfer coefficient  $K_{trans}$  in lung cancer. *PLoS ONE.* 2022;17(3):e0265056.

## Publisher's Note

Springer Nature remains neutral with regard to jurisdictional claims in published maps and institutional affiliations.

**Ready to submit your research? Choose BMC and benefit from:**

- fast, convenient online submission
- thorough peer review by experienced researchers in your field
- rapid publication on acceptance
- support for research data, including large and complex data types
- gold Open Access which fosters wider collaboration and increased citations
- maximum visibility for your research: over 100M website views per year

**At BMC, research is always in progress.**

Learn more [biomedcentral.com/submissions](https://biomedcentral.com/submissions)

